



PERGAMON

Chemical Engineering Science III (IIII) III-III

 Chemical
Engineering Science

www.elsevier.com/locate/ces

Numerical study of mixing of passive and reactive scalars in two-dimensional turbulent flows using orthogonal wavelet filtering

C. Beta^{a,b}, K. Schneider^c, M. Farge^b, H. Bockhorn^{a,*}^a*Institut für Chemische Technik, Universität Karlsruhe (TH), Kaiserstraße 12, 76128 Karlsruhe, Germany*^b*Laboratoire de Météorologie Dynamique du CNRS, Ecole Normale Supérieure de Paris, 24 rue Lhomond, 75231 Paris Cedex 05, France*^c*Laboratoire de Modélisation et Simulation Numérique en Mécanique du CNRS & Centre de Mathématiques et d'Informatique, Université de Provence, 39 rue Joliot-Curie, 13453 Marseille Cedex 13, France*

Received 24 May 2002; received in revised form 11 November 2002; accepted 22 November 2002

Abstract

We present the application of orthogonal wavelet filtering to study mixing and chemical reaction in 2D turbulent flows. We show that the coherent vortices are responsible for the mixing dynamics. Therefore, we perform direct numerical simulation of decaying and statistically stationary homogeneous isotropic 2D turbulence. We split the flow in each time step into coherent vortices represented by few wavelet modes and containing most of the kinetic energy and an incoherent background flow. We quantify the mixing properties of both flow components and demonstrate that efficient mixing of scalars is triggered by the coherent flow, while the influence of the incoherent flow on the mixing corresponds to pure diffusion. These results hold for both passive scalars and reactive scalars with simple and multi-step kinetics.

© 2003 Elsevier Science Ltd. All rights reserved.

Keywords: Fluid dynamics; Simulation; Two-dimensional turbulence; Mixing; Diffusion; Wavelets

1. Introduction

1.1. Background

Mixing is a phenomenon of multiple interests. In chemical industry in particular, mixing is of primordial importance for process control and optimization of chemical reactors. Many industrially relevant reactions take place in homogeneous fluid phase, under turbulent flow conditions, because the mixing properties of turbulent flows are superior to the ones of laminar flows (Ottino, 1990). Problems of industrial mixing are thus closely associated to turbulence (Bockhorn, 1991).

Due to the rapid evolution of computing power over the last decades, numerical simulations have become an important domain of research in turbulence, which provides complementary information in addition to experiments. In direct numerical simulation (DNS) of turbulent flows, where the equations of motion of the fluid are solved on all scales, the

number of degrees of freedom to be computed scales proportionally to Re in two and to $Re^{9/4}$ in three dimensions, Re being the Reynolds number of the flow. For technically relevant flows, whose Reynolds numbers typically range from 10^6 up to 10^{12} , numerical simulations are beyond the computational resources presently available, as long as one does not reduce the number of degrees of freedom. Usually, turbulence models are introduced by splitting the total number of degrees of freedom into, so called, active and passive modes. While the active modes are deterministically computed, the influence of the passive modes onto the active ones is taken into account by computationally less expensive modelling.

The state of the art following this approach is large eddy simulation (LES) (Ferziger, 1995). The splitting is carried out by applying a low-pass filter to the equations of motion and by supposing the large scales to be the active modes while the small scales are assumed to be passive. By resolving the large scales only, LES benefits from the fact that most of the kinetic energy of the flow is confined to small wave numbers. A subgrid scale model is added to the equations of motion to account for the effect of the unresolved modes (small scales) onto the resolved modes (large scales).

* Corresponding author. Tel.: +49-721-608-2120;

fax: +49-721-608-4820.

E-mail address: bockhorn@ict.uni-karlsruhe.de (H. Bockhorn).

In Farge, Schneider, Pellegrino, Wray, and Rogallo (2000) we have shown that the subgrid scales to be modelled have non-Gaussian statistics for the velocity.

For mixing and reacting flows this kind of modelling needs to be extended. For LES, there is numerous work devoted to this problem (e.g. Moin, Pierce, & Pitsch, 2000; Cook & Riley, 1998, Im, Lund, & Ferziger, 1997). Mixing involves scales down to the molecular level. Therefore, the smallest scales of the problem become important, even more if chemical reactions are involved. For the numerical simulation of mixing, the strategy of LES focussed on capturing the large scales, thus runs into conflict with the opposite requirements of the interaction of mixing and chemical reaction that takes place on the sub-filter level and has to be modeled entirely.

1.2. Motivation

The overall aim of this work is to gain some more fundamental insight into the dynamics of mixing in two-dimensional turbulent flows and to use this understanding to develop an efficient method for modelling the mixing of passive and reactive scalars in turbulent flows.

In Gerlinger, Schneider, Falk, and Bockhorn (2000), we numerically studied the role of coherent vortices in the mixing of two-dimensional passive and reactive scalar fields. Basic vortex arrangements and their dynamics, such as the formation of spirals and the merging of co-rotating vortices, were analysed with respect to their mixing properties and found to be mainly responsible for an enhanced diffusion of the scalar fields. For modelling of mixing processes in turbulent flows we should thus rely on a method that stresses the importance of vortex dynamics and coherent structures in the evolution of the flow field.

Recently, a new approach to model turbulent flows, based on the wavelet representation, has been developed (Farge, 1992; Meneveau, 1991; Farge, Schneider, & Kevlahan, 1999). Wavelets are self-similar functions, well localized in both space and scale. They can be considered as basic building units of different function spaces. They allow the decomposition of a function into space, scale, and eventually directions (e.g. Daubechies, 1992; Louis, Maaß, & Rieder, 1998; Mallat, 1997).

Wavelet methods extract the coherent modes by projecting the vorticity field onto a wavelet basis and subsequently thresholding the wavelet modes. This leads to a separation into coherent vortices on the one hand, treated as active modes and computed deterministically in an adaptive wavelet basis, and an incoherent background noise on the other hand, which is to be modelled (Farge & Rabreau, 1988; Farge, 1992). Both parts are multiscale and show a different, clearly distinguished statistical behaviour: the coherent vortices appear to be responsible for the shape of the vorticity probability density function (PDF) which differs from a normal distribution, whereas the incoherent background

has a Gaussian vorticity PDF. The modelling of turbulent flows based on this separation is called coherent vortex simulation (CVS) (Farge et al., 1999), and the separation itself is called CVS filtering. It is well developed for homogeneous isotropic two-dimensional turbulence (Farge et al., 1999), and it has been recently extended to incompressible three-dimensional flows (Farge, Pellegrino, & Schneider, 2001; Schneider, Farge, Pellegrino, & Rogers, 2000). Compressibility effects can be taken into account by decomposing the flow into a potential part and a rotational part using Helmholtz decomposition. The CVS will then be applied to the rotational part while the potential flow will be computed with classical methods (Farge et al., 2002).

The CVS method is built upon extracting the coherent vortices. Bearing in mind the multiscale nature of this decomposition and the clear cut separation of the statistical behaviour of coherent vortices and background flow, there is reason to hope that CVS will constitute a suitable approach for modelling of mixing and chemical reaction. The present work, showing the application of CVS filtering on mixing in non-reactive and reactive two-dimensional flows, is a first step towards extending CVS for mixing problems.

The following section summarizes the considered physical problem. In section three, the wavelet-based CVS filtering and its application to turbulent mixing are introduced, considering both decaying and statistically stationary two-dimensional turbulence. Section four presents and discusses the results of applying the CVS filter to study mixing of passive and chemically reactive scalars with chemical kinetics of different complexity. We examine whether the wavelet representation used for the CVS method is suited for describing, not only the dynamics of turbulent flows, but also the more complex behaviour of mixing and even chemical reactions. We end with giving conclusions and further perspectives in the final section.

2. Considered physical problem

2.1. Two-dimensional turbulent flows

The dynamics of an incompressible and Newtonian flow is described by the *Navier–Stokes equations* (NSE). Without a continuous supply of energy to the flow, the total kinetic energy is decreasing in the course of time due to viscous dissipation (*decaying turbulence*). Statistically stationary turbulence can be obtained if additional energy is supplied by forcing (*forced turbulence*) to compensate dissipation. In vorticity–velocity formulation, including a forcing term, the NSE for a two-dimensional flow take the following form:

$$\partial_t \omega + (\mathbf{v} \cdot \nabla) \omega = \frac{1}{Re} \nabla^2 \omega + \lambda \Psi + F, \quad (1)$$

$$\nabla \cdot \mathbf{v} = 0 \quad (2)$$

with $\mathbf{v} = (u(\mathbf{x}, t), v(\mathbf{x}, t))$ denoting the velocity measured at point $\mathbf{x} = (x, y)$ and at instant t , Ψ the stream function defined

by $\Delta\Psi = \omega$, and λ the strength of the Rayleigh friction term. The Reynolds number Re of the flow is defined as $Re = 2\pi\sqrt{2E}/\nu$ with E the kinetic energy of the flow, 2π the domain size, and ν the kinematic viscosity of the fluid. The energy is supplied by a forcing term F into the equations and, to avoid the accumulation of energy in the large scales due to the inverse energy cascade of 2D turbulence, there is an additional large scale dissipation term $\lambda\Psi$, the so-called Rayleigh friction (Basdevant, Legras, Sadourny, & B eland, 1981).

The vorticity ω is defined as the curl of the velocity and reduces in two dimensions to a pseudo-scalar, perpendicular to the two-dimensional plane of the flow, $\omega = \partial_x v - \partial_y u$. The velocity is obtained from the vorticity applying the Biot–Savart relation, $\mathbf{v} = \nabla^\perp(\nabla^{-2}\omega)$, with $\nabla^\perp = (\partial_y, -\partial_x)$. The vorticity seems the most natural quantity to represent the two-dimensional flow field, because the coherent vortices, that dominate the dynamics of a turbulent flow, appear as localized concentrations of vorticity. Moreover, due to the absence of vortex stretching in two dimensions, $\omega \cdot \nabla\mathbf{v} = 0$, the NSE in vorticity–velocity formulation take the particularly simple form of a scalar valued transport equation for vorticity.

The problem formed by the system of Eqs. (1) and (2) is completed by appropriate initial and boundary conditions. In this work, the computational domain is a 2π quadratic box $\Omega = [0, 2\pi] \times [0, 2\pi]$ where we impose periodic boundary conditions in order to have maximal symmetry (Frisch, 1995). Thus, the set of all flow realizations corresponds to the idealized case of homogeneous, isotropic turbulence. The initial conditions are specified in Section 4.

Standard numerical schemes are employed to integrate the Navier–Stokes equations and the convection–diffusion–reaction equations discussed below. For the time discretization we use a semi-implicit second-order finite difference scheme consisting of an Euler backwards step for the viscous term and an Adams–Bashforth extrapolation for the convective term. The space discretization is carried out using a pseudo-spectral method, computing spatial derivatives as well as the vorticity evolution in Fourier space, and the non-linear convective term in physical space (see Schneider, Kevlahan, and Farge (1997) and for a more complete discussion of the numerical schemes Canuto, Hussaini, Quaternioni, and Zang (1988)).

The Fourier transform of the velocity field $\mathbf{v}(\mathbf{x}, t)$ is defined as

$$\hat{\mathbf{v}}(\mathbf{k}, t) = \frac{1}{4\pi^2} \int_{\Omega} \mathbf{v}(\mathbf{x}, t) e^{-i\mathbf{k}\cdot\mathbf{x}} d\mathbf{x}, \quad (3)$$

where $\mathbf{x} = (x, y)$, $i = \sqrt{-1}$, and $\mathbf{k} = (k_x, k_y)$ denotes the wavenumber vector. Following Parseval’s identity, the specific kinetic energy of the flow can be defined equivalently in physical or spectral space,

$$E(t) = \frac{1}{2} \frac{1}{4\pi^2} \int_{\Omega} |\mathbf{v}(\mathbf{x}, t)|^2 d\mathbf{x} = \frac{1}{2} \int_{\Omega} |\hat{\mathbf{v}}(\mathbf{k}, t)|^2 d\mathbf{k}. \quad (4)$$

The distribution of energy over k in spectral space is called the isotropic *energy spectrum* of a turbulent flow, defined as

$$E(k, t) = \frac{1}{2} \int_{|\mathbf{k}|=k} |\hat{\mathbf{v}}(\mathbf{k}, t)|^2 d\mathbf{k} \quad (5)$$

with $k = |\mathbf{k}| = \sqrt{k_x^2 + k_y^2}$ the modulus of the wavenumber vector. Note that energy equipartition corresponds to $E(k, t) \sim k$ due to the fact that we are integrating over concentric circles in wavenumber space. In the same way we may define the total *enstrophy*, based on the vorticity representation of the flow field,

$$Z(t) = \frac{1}{2} \frac{1}{4\pi^2} \int_{\Omega} |\omega(\mathbf{x}, t)|^2 d\mathbf{x} = \frac{1}{2} \int_{\Omega} |\hat{\omega}(\mathbf{k}, t)|^2 d\mathbf{k} \quad (6)$$

with a corresponding enstrophy spectrum

$$Z(k, t) = \frac{1}{2} \int_{|\mathbf{k}|=k} |\hat{\omega}(\mathbf{k}, t)|^2 d\mathbf{k}, \quad (7)$$

that is related to the spectral energy distribution according to

$$Z(k, t) = k^2 E(k, t). \quad (8)$$

2.2. Mixing

We consider the mixing of non-reactive (passive) and chemically reactive (active) scalars in homogeneous fluid media. As stated above, the work is confined to incompressible flows. Furthermore, all transport coefficients are supposed to be constant and chemical reactions are treated in the isothermal limit, so that the temperature equation needs not to be considered.

In this case, the dynamics of a scalar i in a flow field is described by the convection–diffusion equation,

$$\partial_t c_i + \mathbf{v} \cdot \nabla c_i - \frac{1}{Sc_i Re} \nabla^2 c_i = -r, \quad (9)$$

where $c_i = c_i(\mathbf{x}, t)$ denotes the concentration of species i with Schmidt number Sc_i and Re the Reynolds number of the flow. The Schmidt number is defined as the ratio $Sc_i = \nu^*/D_i^*$ with ν^* the kinematic viscosity of the fluid and D_i^* the molecular diffusivity of the species i . Here, the superscript $*$ indicates the dimensionalized form of physical quantities (for notation of physical quantities and their non-dimensionalized forms see Appendix C). For passive scalars the source term r is zero, while for active scalars the term r represents the chemical reaction rate for the reactive species in the flow. For a second-order reaction of type



between two species A and B, the source term is of the form $r = Da c_A c_B$ with a Damk ohler number of $Da = k^* t_0^* c_0^*$ (k^* denoting the reaction rate coefficient of the second order chemical reaction). In this case, (9) holds for $i = A, B$. Besides, we define the integral reaction rate $R(t)$ as

$$R(t) = \frac{1}{4\pi^2} \int_{\Omega} r(\mathbf{x}, t) d\mathbf{x}. \quad (11)$$

Before any chemical reaction can take place, the initially segregated species need to be mixed down to a molecular level. Thus, the integral reaction rate can be regarded as a measure of the degree of mixing of the reactants.

Furthermore, in analogy to the kinetic energy, we define a corresponding scalar “energy” (Lesieur, 1997) based on the second moment of the concentration field,

$$E_C(t) = \frac{1}{2} \frac{1}{4\pi^2} \int_{\Omega} |c(\mathbf{x}, t)|^2 d\mathbf{x} \quad (12)$$

and call the isotropic spectral distribution of this quantity

$$E_C(k, t) = \frac{1}{2} \int_{|\mathbf{k}|=k} |\hat{c}(\mathbf{k}, t)|^2 d\mathbf{k} \quad (13)$$

the *scalar spectrum*.

In a fluid at rest, a passive scalar spreads according to the law of molecular diffusion. For strong concentration gradients, that is, at the interface of initially segregated species, molecular diffusion is fast at early times but becomes very slow as time increases. This slowing down is the major issue of most mixing problems. The only way to compensate for it and to speed up the mixing is to increase the interfacial area. Thus, one can distinguish two types of interacting mechanisms that form a mixing process. On the one hand, there is convective mixing, during which an initially compact region of the fluid is stretched and folded throughout space (*macro-mixing*). On the other hand, molecular diffusion causes the mixing species to cross the interfaces of initial segregation and to mix on a molecular level (*micro-mixing*) (Ottino, 1989).

In order to characterize macro-mixing, the stretching efficiency of the flow or, more precisely, the production of concentration gradient needs to be quantified. To this end, inspired by Protas, Babiano, and Kevlahan (1999), Lapeyre, Klein, and Hua (1999); Lapeyre, Hua, and Klein (2000), we define an instantaneous local relative production rate of concentration gradient, $\gamma = \frac{1}{2} \eta s \cos 2\alpha$, which depends on the magnitude of the concentration gradient vector, $\eta = |\nabla c|$, the elements of the strain tensor, $s = \sqrt{s_{11}^2 + s_{12}^2}$, and the angle α between the concentration gradient vector and the compressing eigenvector of the strain tensor (for a detailed derivation of this quantity see Appendix A). As a measure for the overall macro-mixing, we introduce the *total production rate of scalar gradient* as the integral of the local quantity γ ,

$$\Gamma(t) = \int_{\Omega} \gamma(\mathbf{x}, t) d\mathbf{x}. \quad (14)$$

Another global measure to quantify the quality of mixing, the most common one in fact, is the time evolution of the *variance* of the concentration field (Corrsin, 1964),

$$\sigma^2(t) = \int (c(t) - \bar{c})^2 d\mathbf{x} \quad (15)$$

with \bar{c} the constant mean concentration. The variance stays constant during macro-mixing but decreases when micro-mixing takes place. If mixing is due to diffusion

only, the asymptotic behaviour of the variance decay is exponential (Corrsin, 1964), $\sigma^2(t) \sim \exp(-2t/t_0)$, with a mixing time scale t_0 proportional to the Schmidt number. Following Flohr and Vassilicos (1997), Gerlinger et al. (2000), we will consider, instead of the instantaneous variance, the time evolution of the difference $\sigma^2(0) - \sigma^2(t)$. In this case, one expects a time evolution of $(\sigma^2(0) - \sigma^2(t))$ proportional to \sqrt{t} for pure diffusion (Flohr & Vassilicos, 1997). If mixing is enhanced by the stretching and folding of fluid filaments, the decay of the variance will depart from the \sqrt{t} -law, and then corresponds to an accelerated, so-called anomalous diffusion.

3. CVS filtering and its application to mixing

3.1. Wavelets and turbulence

Wavelets (Grossmann & Morlet, 1984) have been recently introduced into turbulence research (Farge & Rabreau, 1988; Farge, 1992; Meneveau, 1991). For a thorough mathematical treatment of wavelet theory the reader is referred to standard textbooks such as Daubechies (1992), Mallat (1997), Louis et al. (1998). The use of wavelet techniques in turbulence is motivated mainly by the need to overcome the limitations of the Fourier representation which requires stationarity and homogeneity of the flow (Batchelor, 1953). On the one hand, wavelets allow to analyse a flow field in terms of both space and scale, thus providing a unified approach able to link the predictions of the present statistical theory, based on Fourier space representation, and intermittent phenomena, such as the formation of coherent vortices observed in physical space. On the other hand, due to the matching between the multiscale character of turbulence and of the wavelet representation, wavelets allow elegant decompositions of turbulent flow fields, extracting most of the localized coherent structures (and a large part of the kinetic energy) with only very few strong modes of the wavelet representation.

In this article, we apply a non-linear wavelet filter to turbulent flow fields and investigate the effect of this filtering on the mixing properties of the flow with regard to passive and chemically active scalar fields. The filtering procedure is inspired by the wavelet-based Coherent Vortex Simulation, a method for computation of fully-developed turbulent flows (Farge et al., 1999; Farge et al., 2001; Farge & Schneider, 2001). We therefore call it CVS filtering.

3.2. CVS filtering

We briefly recall the algorithm introduced in Farge et al. (1999). The CVS filtering consists of three consecutive steps:

Decomposition: By means of a two-dimensional multiresolution analysis (MRA) (Daubechies, 1992; Mallat, 1997)

we expand the vorticity field $\omega(x, y)$ with resolution $N = 2^{2J}$ into an orthogonal wavelet series

$$\omega(x, y) = \bar{\omega}_{0,0,0} \phi_{0,0,0}(x, y) + \sum_{j=0}^{J-1} \sum_{i_x=0}^{2^j-1} \sum_{i_y=0}^{2^j-1} \sum_{\mu=1}^3 \tilde{\omega}_{j,i_x,i_y}^{\mu} \psi_{j,i_x,i_y}^{\mu}(x, y) \quad (16)$$

with

$$\phi_{j,i_x,i_y}(x, y) = \phi_{j,i_x}(x) \phi_{j,i_y}(y) \quad (17)$$

and

$$\psi_{j,i_x,i_y}^{\mu} = \begin{cases} \psi_{j,i_x}(x) \phi_{j,i_y}(y) & \text{for } \mu = 1, \\ \phi_{j,i_x}(x) \psi_{j,i_y}(y) & \text{for } \mu = 2, \\ \psi_{j,i_x}(x) \psi_{j,i_y}(y) & \text{for } \mu = 3. \end{cases} \quad (18)$$

Due to the nature of wavelets, this expansion corresponds to a decomposition both in space and scale (in this case ranging from the largest scale $l_{\max} = 2^0$ down to the smallest scale $l_{\min} = 2^{1-J}$). The functions $\psi_{j,i}$ and $\phi_{j,i}$ denote the one-dimensional wavelet and the corresponding scaling function, respectively. The wavelet and scaling coefficients are $\tilde{\omega}_{j,i_x,i_y}^{\mu} = \langle \omega, \psi_{j,i_x,i_y}^{\mu} \rangle$ and $\bar{\omega}_{0,0,0} = \langle \omega, \phi_{0,0,0} \rangle$ with $\langle f, g \rangle = \int f(\mathbf{x})g(\mathbf{x})d\mathbf{x}$. For the separations in the present article we use a fast wavelet transform algorithm with Battle–Lemarié spline wavelets of order six, which is a $\mathcal{O}(N \log N)$ process because in this case the fast convolutions are performed using FFT-techniques (Mallat, 1997).

Thresholding: By a non-linear thresholding with $\varepsilon_T = (2\langle \omega^2 \rangle \log_e N)^{1/2}$, N denotes the number of grid points and $\langle \omega^2 \rangle$ the variance of the vorticity field, the wavelet coefficients of the vorticity field are split into two parts: a small fraction with $|\tilde{\omega}| > \varepsilon_T$ containing the wavelet coefficients of what we call the *coherent vorticity*, and a large fraction, the *incoherent vorticity*, with all the remaining coefficients having a modulus of $|\tilde{\omega}| \leq \varepsilon_T$.

The choice of ε_T is based on theorems by Donoho (Donoho, 1993; Donoho & Johnstone, 1994) on the use of wavelet thresholding to obtain min–max estimators for denoising of signals with inhomogeneous regularity. Thus, we define the coherent vortices as part of the vorticity field with non-normal statistics and separate them from the incoherent vorticity, the PDF of which resembles a normal distribution.

Reconstruction: By inverting decomposition (16), the coherent and incoherent vorticity fields can be reconstructed using the two sets of coefficients obtained by non-linear filtering. Because the coherent and incoherent vorticity fields are orthogonal to each other, the total enstrophy Z equals the sum of coherent and incoherent enstrophies, $Z = Z_C + Z_I$. The velocity fields, computed from the vorticities by applying the Biot–Savart relation, are only approximately orthogonal and thus $E = E_C + E_I + \varepsilon$ with $\varepsilon \ll E$ (for further explanations see Farge et al., 1999).

3.3. Application to study mixing

The application of the wavelet-based CVS filtering to study the mixing of a scalar quantity in a turbulent flow is summarized by the scheme in Fig. 1. It comprises essentially three different elements:

- **DNS of the flow field:** The time evolution of the vorticity field of the flow is computed by DNS using a standard pseudo-spectral code. This yields a reference run for comparison with the filtered results.
- **CVS filtering at each time step:** Simultaneously with the computation of the flow evolution, the vorticity field is split at each time step into its coherent and incoherent parts applying the above explained CVS filtering. After having filtered the vorticity fields, the corresponding velocity fields are computed at each instant from all three vorticity fields (the total, the coherent, and the incoherent ones).
- **Time evolution of the scalar fields:** At each time step, the coherent, the incoherent, and the total velocity fields are used to advect the non-reactive or reactive scalars. More precisely, the convection–diffusion equations (9) of the scalars are solved three times: using the total velocity field in order to compute a reference case ($\mathbf{v} = \mathbf{v}_T$), using the coherent velocity ($\mathbf{v} = \mathbf{v}_C$) to investigate whether the retained modes contain enough information for correctly computing the mixing process, and using the incoherent velocity ($\mathbf{v} = \mathbf{v}_I$) to learn more about the nature of the discarded modes.

4. Results and discussion

In the following section, we present results derived from the application of CVS filtering to mixing problems in fully developed two-dimensional turbulent flows. First, the initial conditions and simulation parameters are introduced. Then we apply CVS filtering to a freely decaying turbulent flow and study the mixing of passive scalars and of chemically active species with second order kinetics. Finally, we apply the same method to a statistically stationary turbulent flow and consider mixing of active scalars following multi-step kinetics.

4.1. Initial conditions and parameters

4.1.1. Vorticity

As initial condition, for the vorticity of the decaying and the statistically stationary turbulent flows, we choose fully developed turbulent fields, which are shown in the upper half of Fig. 2. They are generated by integration of the 2D Navier–Stokes equations during several eddy turnover times, starting from a homogeneous isotropic random vorticity field with Gaussian probability distribution and given correlation (Farge et al., 1999).

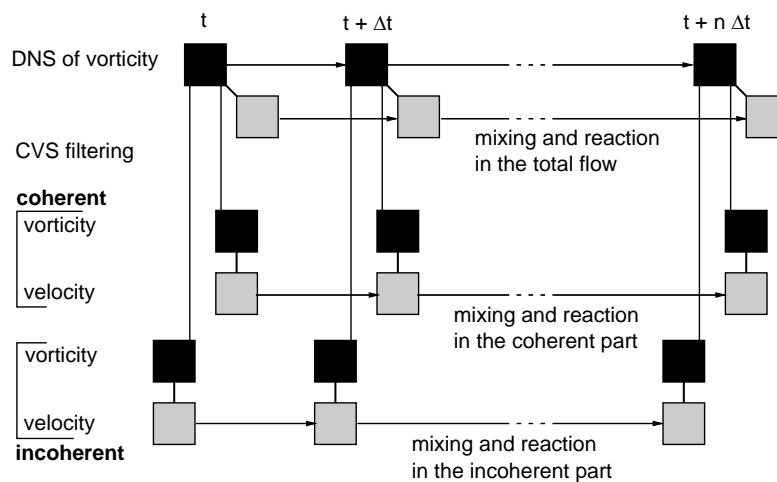


Fig. 1. Application of CVS filtering to study mixing and reaction in turbulent flows: flow chart of the numerical integration. The black squares represent the vorticity fields and the grey squares the velocity fields.

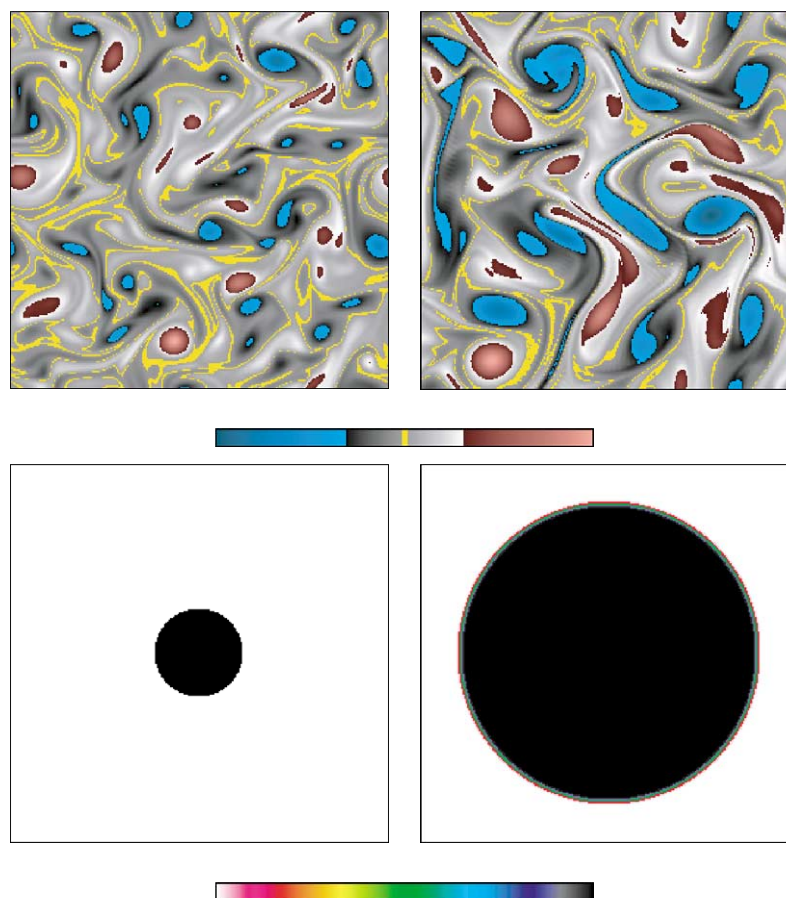


Fig. 2. Initial conditions: vorticity (top) of the decaying (left) and the statistically stationary turbulent flow (right), and concentration (bottom) of the passive (left) and the reactive scalar fields (right).

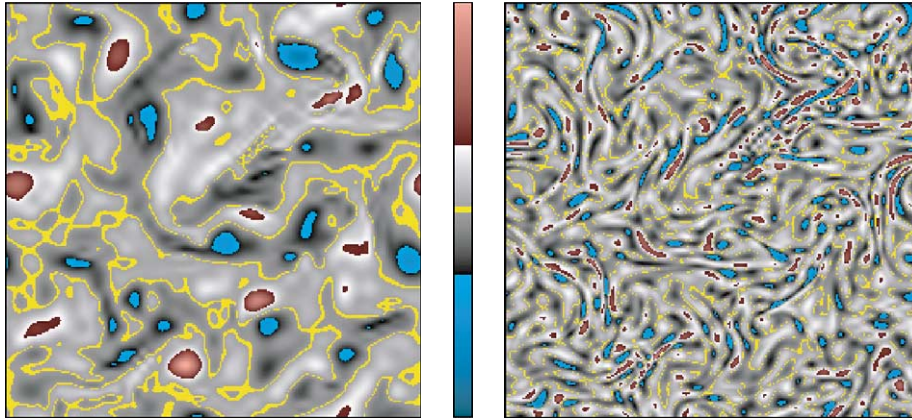


Fig. 3. CVS filtering of the initial vorticity field (Fig. 2 top, left): coherent (left) and incoherent part (right).

4.1.2. Concentration

Throughout this article, we normalize concentration fields between zero and one. Moreover, due to the isotropic nature of the flow, we choose circular initial geometries for the scalar fields.

Fig. 2 (bottom, left) shows the initial condition for the passive scalar. We start with total segregation between a centred circular spot of maximal concentration (with a diameter such that the mean concentration of the field equals 0.043) and a surrounding region of zero concentration.

For the second order and autocatalytic reactions, we again start with a circle for component A (Fig. 2, bottom right hand side), this time setting the diameter such that the mean concentration of A is 0.5. Besides, we smoothen the initial step-profile of the concentration field using a standard error function in order to avoid Gibbs oscillations induced by the Fourier discretization of the pseudo-spectral code. The choice of an error function profile can be physically interpreted as a step-profile having been exposed to diffusion, because the standard error function is solution of the diffusion equation. The initial condition of component B in the second order and autocatalytic reactions is given by $c_B(\mathbf{x}, t = 0) = 1 - c_A(\mathbf{x}, t = 0)$.

4.1.3. Parameters

All simulations discussed in the present paper were carried out with a spatial resolution of $\Delta x = \Delta y = (2\pi/256)$, corresponding to a number of $N = 256^2$ grid points. The kinematic viscosity is $\nu^* = 9.9 \times 10^{-4} \text{ m}^2 \text{ s}^{-1}$. The Reynolds number, according to the above given definition, is about 2800 for the decaying turbulent flow and 7800 for the statistically stationary turbulent flow, based on the kinetic turbulent energy and the size of the domain. The Schmidt number for all scalars is $Sc = 1$.

The statistically stationary turbulent flow is computed using a standard Fourier forcing where energy is supplied at wavenumber $k = 4$ with an amplitude of one. The parameter λ in the Rayleigh dissipation term of Eq. (1) is chosen as $\lambda = 1.0$ (Legras, Santangelo, & Benzi, 1988).

Table 1

Compression rate, energy, and enstrophy for CVS filtering of the initial vorticity field

# Coefficients	Total	65536	(100%)
	Coherent	566	(0.9%)
	Incoherent	64970	(99.1%)
Energy	Total	0.0974	(100%)
	Coherent	0.0967	(99.3%)
	Incoherent	6.5526×10^{-4}	(0.7%)
Enstrophy	Total	2.2046	(100%)
	Coherent	2.0531	(93.1%)
	Incoherent	0.1515	(6.9%)

The time step for all simulations is set to $\Delta t = 5 \times 10^{-4}$. The mixing processes in the decaying turbulent flow are computed during 10,000 time steps, corresponding to 10 initial eddy turnover times. The eddy turnover time is defined as $\tau = 1/\sqrt{2Z_0}$ with Z_0 the initial enstrophy. The mixing in the statistically stationary flow with the autocatalytic reaction is computed during 80,000 time steps, corresponding to 176 eddy turnover times.

The computations have been performed on PC clusters with Intel Pentium III processors, 1400 MHz. A simulation for the mixing of a passive scalar required about 16 MB of memory and one time step took 2.4 s. Thus, the total computing time for one simulation (10,000 time steps) was about 6 : 40 h.

4.1.4. CVS filtering

To illustrate the CVS filtering of the vorticity field, that is carried out at each time step of the flow evolution, we study here in some detail the influence of the filtering for the initial condition of the decaying turbulent flow.

To this end, the flow field is projected onto an orthogonal wavelet basis using the two-dimensional MRA introduced in Section 3.2. Thresholding of the wavelet coefficients and subsequent reconstruction from the two sets of coefficients yields the coherent and incoherent vorticity fields shown in Fig. 3.

Compression rates, energy, and enstrophy for the filtered fields are summarized in Table 1. These values demonstrate

Table 2
Statistical properties of the total, the coherent, and the incoherent vorticity fields

	Definition	Total	Coherent	Incoherent
Second moment	$M_2 = (1/N) \sum_i \omega_i^2$	5.0	4.7	0.3
Third moment	$M_3 = (1/N) \sum_i \omega_i^3$	4.0	4.3	0.0
Fourth moment	$M_4 = (1/N) \sum_i \omega_i^4$	132	118	0.4
Fifth moment	$M_5 = (1/N) \sum_i \omega_i^5$	398	378	0.0
Sixth moment	$M_6 = (1/N) \sum_i \omega_i^6$	7208	5946	1.0
Skewness	$S = M_3/M_2^{3/2}$	0.36	0.42	0.0
Flatness	$F = M_4/M_2^2$	5.3	5.4	3.5

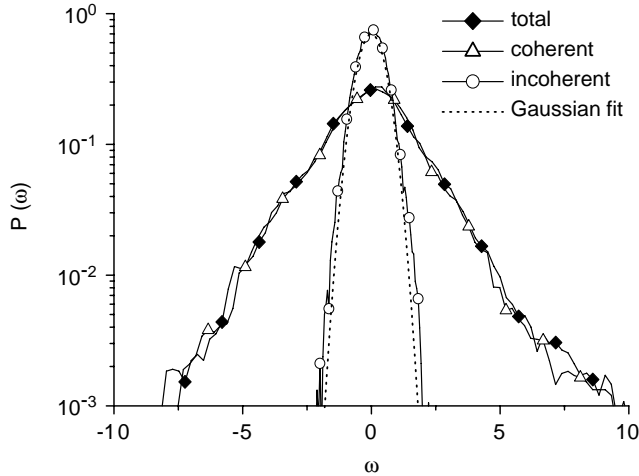


Fig. 4. PDF of the total initial vorticity field and of its coherent and incoherent parts.

the efficiency of wavelet compression for fully developed turbulent flow fields. On the one hand, the coherent vorticity field is made of only 0.9% of the wavelet modes but contains almost all kinetic energy (99.3%) and most of the enstrophy (93.1%). Thus, all important information concerning the dynamical behaviour of the flow is captured in the coherent part, which is confirmed also by visually comparing the local structure of the coherent and the total fields. On the other hand, the incoherent field, reconstructed from the remaining 99.1% of the wavelet modes, looks like a homogeneous random noise without any localized coherent structures and contains almost no kinetic energy and only very little enstrophy.

These observations may be further quantified by looking at the statistical properties of the filtered fields. The statistical moments of the total, coherent, and incoherent fields are listed in Table 2. The incoherent part shows a statistical behaviour similar to a Gaussian normal distribution with moments of uneven order being zero and a flatness of three. The coherent part is non-Gaussian and reproduces closely the statistics of the total vorticity field. This is summarized by the PDFs of all three fields shown in Fig. 4. The PDF of the incoherent part, plotted in a log–lin scale, is of approximately parabolic shape, as expected for a Gaussian

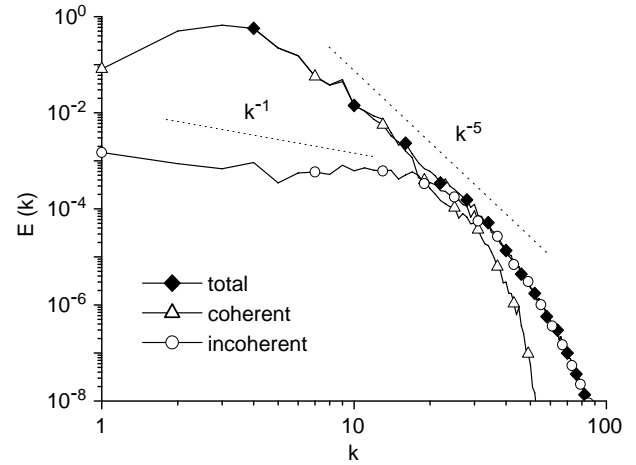


Fig. 5. Energy spectrum of the total initial turbulent flow and of its coherent and incoherent parts.

distribution, and the PDF of the coherent part is stretched exponential and superposes well with the PDF of the total field.

The energy spectrum for the CVS filtering is shown in Fig. 5. Apart from the high-wavenumber region, corresponding to the dissipative range, the total energy spectrum is well reproduced by the spectrum of the coherent part with a k^{-5} power law behaviour in the inertial range. For the incoherent part we find a k^{-1} behaviour of the energy spectrum corresponding to an equidistribution of enstrophy, which scales as k^{+1} since $Z(k) = k^2 E(k)$ (cf. Eq. (8)). Thus, the incoherent vorticity field is decorrelated. Moreover, both the coherent and the incoherent parts of the flow are of multiscale nature.

These results are in close correspondence with the results of similar filtering reported in Farge et al. (1999).

4.2. Mixing of a passive scalar (decaying turbulence)

Starting from the initial condition shown in Fig. 2, we compare the mixing of a passive scalar in the total turbulent flow and in its coherent and incoherent parts. Fig. 6 shows the passive scalar field after five time units of the flow evolution for the total flow, the coherent part, and the incoherent part. Although the coherent part is made of only

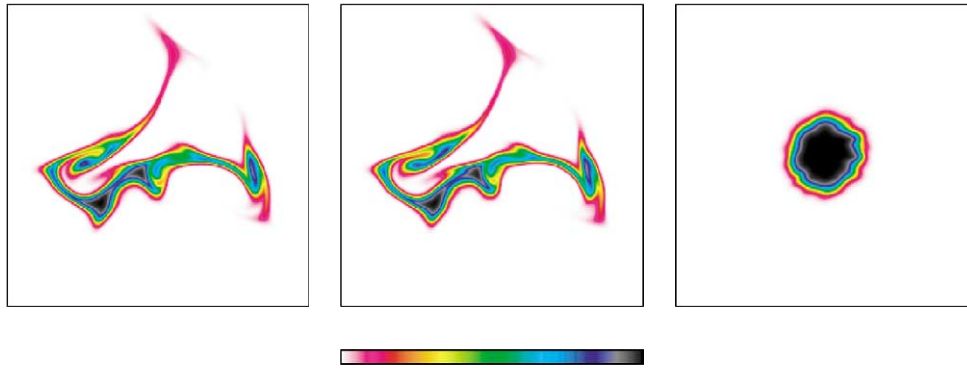


Fig. 6. Passive scalar field at $t = 5$, advected by the total flow (left), the coherent flow (middle), and the incoherent flow (right).

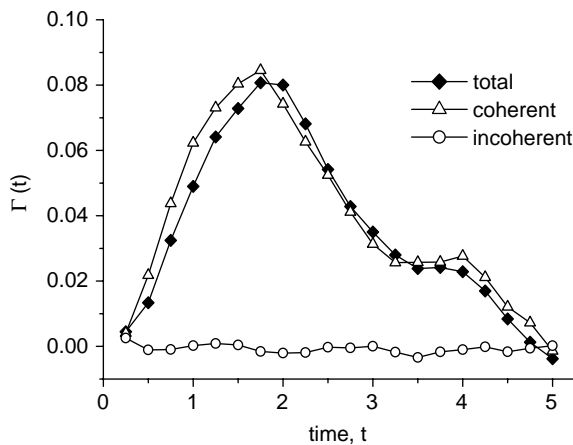


Fig. 7. Time evolution of the production rate of scalar gradient.

0.9% N of the wavelet modes, the evolution of the scalar field computed from the coherent part (Fig. 6, middle) looks almost exactly like the one computed from the total flow (Fig. 6, left), whereas the scalar field in the incoherent part (Fig. 6, right) looks completely different and seems to be affected by diffusion only. Thus, the coherent part reproduces the mixing properties of the total turbulent flow to a nearly complete extend and only a close comparison reveals small differences between the two scalar fields.

The close matching of the scalar fields in the total flow and in the coherent part is confirmed when taking into account the above introduced measures for the overall mixing process. In Fig. 7, the time evolution of the scalar gradient production rate is shown for the total flow in comparison with its coherent and incoherent parts. Because the scalar gradient production rate is reflecting mostly the stretching and folding of the interface of the segregated, non-mixed regions, the close matching of the graphs for the total flow and the coherent part confirms that the convective macro-mixing dynamics of the flow is almost completely captured in the 0.9% N wavelet modes constituting the coherent part, while the incoherent part of the flow contains no significant contribution to the convective transport in the flow. Moreover, the evolution of the variance of the scalar field, plotted in

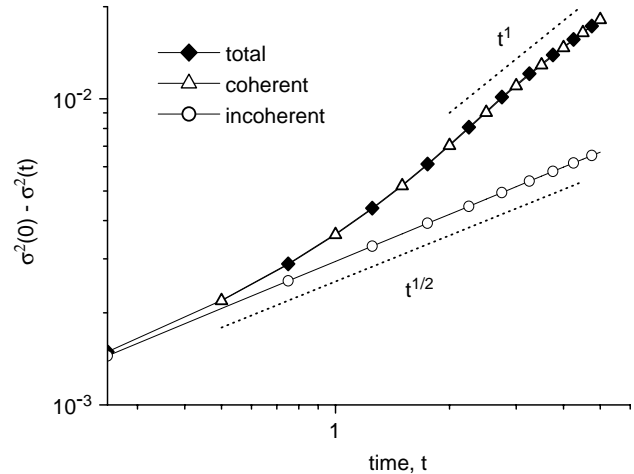


Fig. 8. Time evolution of the difference between initial and instantaneous variances for the passive scalar.

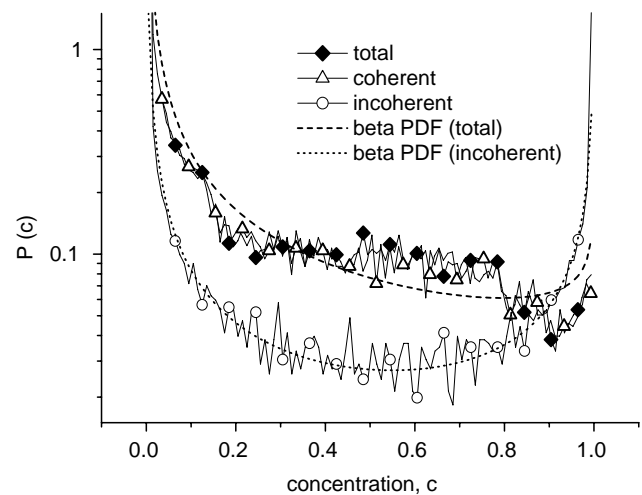


Fig. 9. PDFs of the concentration for the passive scalar at $t = 5$.

Fig. 8 as the difference between the initial and the instantaneous variances in a double logarithmic plot, indicates that not only the convective transport but also the overall mixing in the total flow is closely reproduced by the coherent part. Besides, from this plot we are also able to

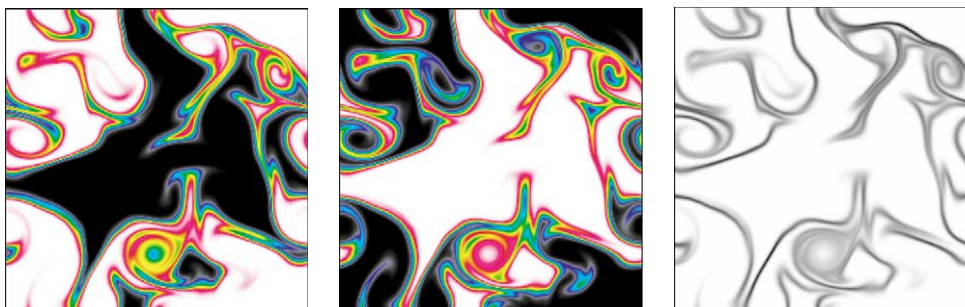


Fig. 10. Reactive scalars A and B, and reaction rate for the second-order reaction at $t = 5$ in the coherent part of the flow: A (left), B (middle), reaction rate (right).

characterize the nature of the mixing dynamics in the incoherent part of the flow. We find in the double logarithmic plot a \sqrt{t} behaviour, as predicted by theory for a purely diffusive behaviour (Flohr & Vassilicos, 1997).

Furthermore, it is important to point out that the global time scale of the mixing process is strongly dependent on the Schmidt number Sc_i of the scalar quantity. For the approximation of the global mixing time scales and their dependence on the Schmidt number see Gerlinger et al. (2000).

Fig. 9 shows the PDF of the passive scalar field in the total flow and in the coherent and incoherent parts at $t = 5$. Here also, the PDF confirms that the concentration field in the coherent part shows good agreement with the concentration field in the total flow. Moreover, the PDFs of the concentration in the total flow and in the incoherent part are fitted with the respective β -PDFs (the fit for the concentration PDF of the coherent part is omitted since it superposes exactly with the fit for the total flow). For the computation of β -PDFs we refer to Appendix B. Obviously, the PDF of the concentration field in the incoherent part of the flow is fitted very well by a β -PDF, much better than the concentration PDF in the total flow. This might be of importance for future modelling of the mixing process in the incoherent part of the flow.

4.3. Mixing of reactive scalars (decaying and statistically stationary turbulence)

4.3.1. Second order reaction (decaying turbulence)

The above investigation for a passive scalar is now extended to the mixing of two initially segregated reactive scalars linked by a second-order reaction of type



(for the initial condition see Fig. 2). Fig. 10 shows the reactive scalar fields and the reaction rate computed by integrating the convection–diffusion–reaction equations over five units of time using only the coherent part of the flow. We refrain from printing the same fields computed from the total flow since the visual differences are as small as they were for the passive scalar (cf. Fig. 6).

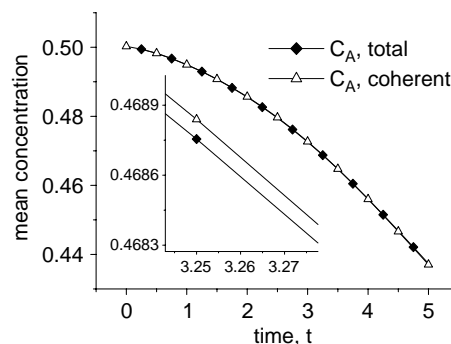


Fig. 11. Time evolution of the mean of concentration (reactive scalar A) for the second-order reaction. The inset shows a zoom around $t = 3.26$ and $\bar{c} = 0.4686$.

The reaction rate (Fig. 10, right) shows clearly that chemical reaction takes place at the interface between A and B. Here, due to steep concentration gradients, we observe diffusive mixing of the two components on a molecular level which is required for a chemical reaction to take place. This process is particularly efficient where strong scalar gradients are produced due to stretching and folding of the interface under the effect of vortices. Note for instance the formation of a spiral in the lower middle part of Fig. 10, leading to an enhanced diffusive mixing and subsequent reaction of the components inside a vortex. A systematic discussion of elementary vortex arrangements and their mixing properties for different initial conditions of the concentration fields and varying Damköhler numbers can be found in Gerlinger et al. (2000).

As for the passive scalar, we quantify the difference in the mixing dynamics of the total flow and the coherent part by tracing the time evolution of some parameters related to the mixing and reaction process of the two components. The mean concentration, shown in Fig. 11 for component A, decreases due to reaction and superposes perfectly for the reaction in the total flow and in the coherent part. The integral reaction rate (Fig. 12) rises linearly and approaches a saturation value (cf. other results from literature for the reaction of scalars with Schmidt number $Sc = 1.0$, e.g. in

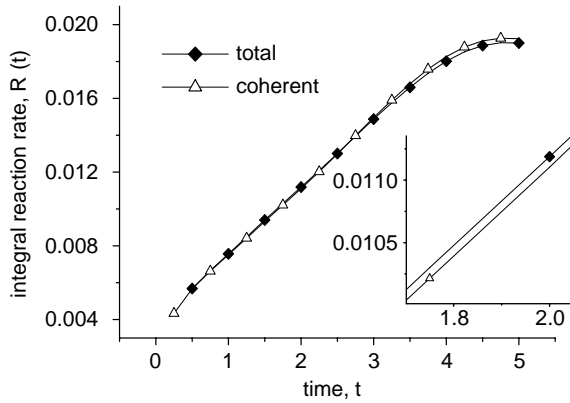


Fig. 12. Time evolution of the integral reaction rate for the second-order reaction. The inset shows a zoom around $t = 1.9$ and $R = 0.0105$.

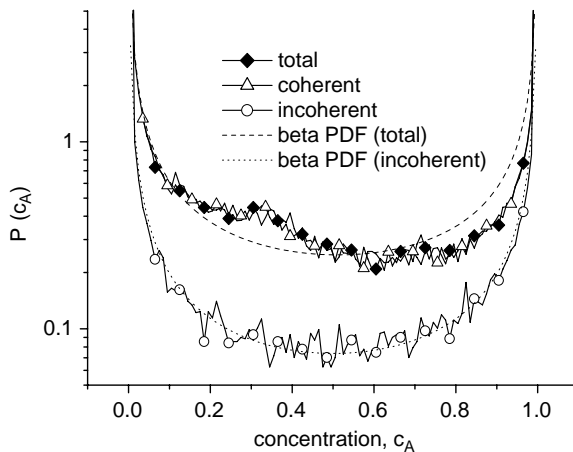


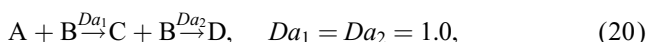
Fig. 13. PDFs of concentration (reactive scalar A) for the second-order reaction at $t = 5$.

Gerlinger et al., 2000). Only towards the end, a difference emerges that remains small and constant.

The PDFs of concentration A in the total flow and in the coherent and incoherent parts at $t = 5$ are shown in Fig. 13. As for the passive scalar, the PDFs for the concentrations in the total flow and the coherent part superpose very well. Again, the concentration PDF in the incoherent part can be closely fitted using a β -PDF. Thus, it seems that also for reactive scalars the mixing process in the incoherent part of the flow may be modelled using a β -PDF for describing the concentration field.

4.3.2. Multi-step reaction (statistically stationary turbulence)

In order to test the CVS filtering for a more complex case, we have chosen the autocatalytic reaction



taking place in a statistically stationary turbulent flow. Again, we compute the mixing and reaction process by solving the convection–diffusion–reaction equations using both the total flow and its coherent part, starting from the same initial condition for A and B (Fig. 2), while there is no C in the medium at time $t = 0$. In Fig. 14, we show the scalar fields A (top), B (middle), and C (bottom) at three selected time steps. As for the second order reaction, we only show the scalar fields computed from the coherent part, because there is no significant difference to the ones computed from the total flow. At the beginning, the scalar fields A and B are of nearly complementary shapes due to the initial configuration. At $t = 17.5$, it is already obvious that the total amount of A is decreasing quicker than the amount of B . Component C emerges at the interface between regions of A and B , where there is diffusive mixing due to steep concentration gradients and subsequent reaction.

The evolution of the mean concentrations (Fig. 15) and the integral reaction rates (Fig. 16) are exactly superposed for the total flow and the coherent part. The mean concentrations of the reactive components follow the reaction scheme: A and B decrease monotonically with a certain delay for B due to the catalytic character of the first step. The amount of C first increases with the consumption of A and attains its maximum before the moment when the second step (reaction of B and C to D) starts to dominate the composition of the medium. The integral reaction rates reflect this evolution. First, the reaction rate of the catalytic step reaches its maximum at about $t = 4$, when A and B are already well mixed and before the time where the concentration of A decreases rapidly. Shortly afterwards, the rate of the second step goes through a maximum, which is reached at the same time when there is a maximal amount of C in the medium.

In Figs. 17 and 18, we finally show some statistical properties of the scalar fields at $t = 17.5$. The scalar energy spectra (Fig. 17) are plotted for component A . The spectrum derived from the mixing in the coherent part fits well onto the spectrum of the total flow. Moreover, we find a scaling law in k^{-7} for large wavenumbers, as predicted by the phenomenological theory (Lesieur, 1997). The PDFs of all three scalar fields (Fig. 18) also look satisfyingly similar for mixing in the total flow and in the coherent part. At $t = 17.5$, most of A is already consumed by the catalytic step of the reaction (maximum of the PDF of A at small values), while there are still larger amounts of C and B in the medium (maximum of the respective PDFs at larger values).

5. Conclusion

In this work, we presented results from numerical simulations of mixing of passive and chemically active scalars in decaying and statistically stationary two-dimensional, isotropic turbulence. In particular, we applied to the flow an orthogonal discrete wavelet filter, the CVS filter, and studied its effect on the mixing and reaction process.

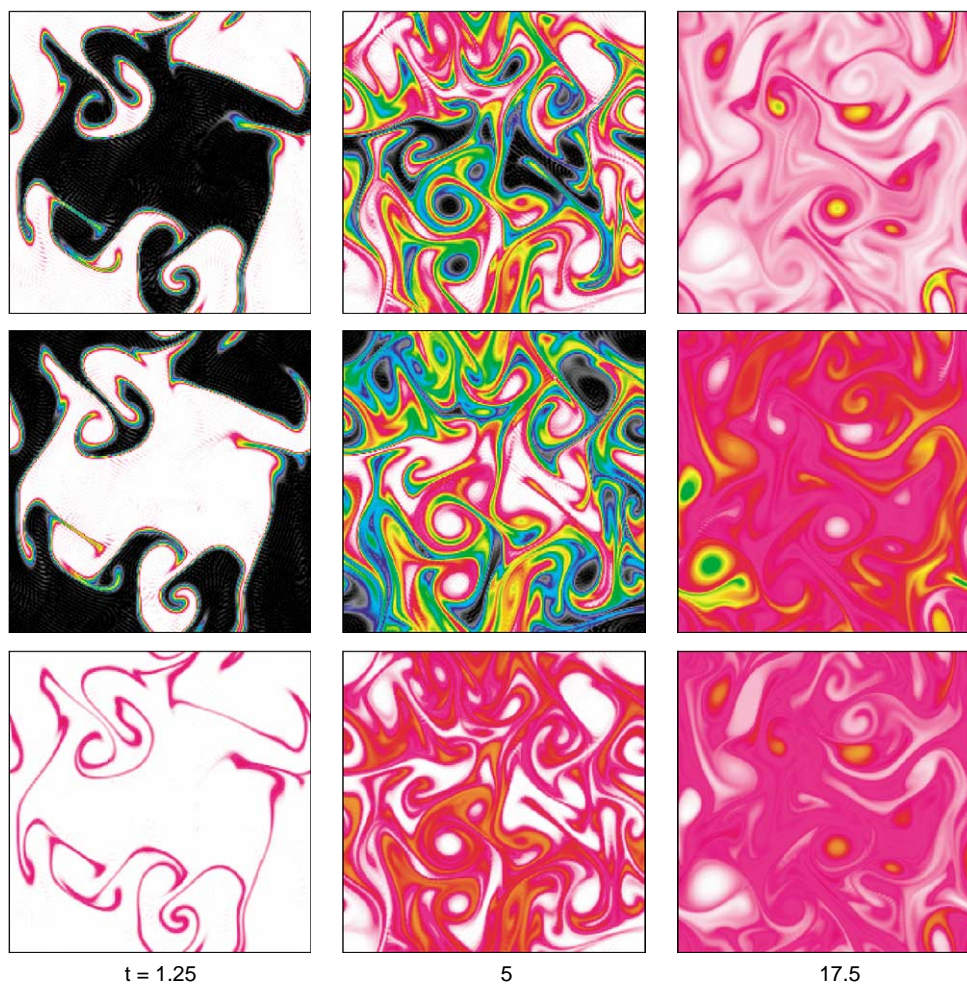


Fig. 14. Time evolution of reactive scalars A (top), B (middle), and C (bottom) for the autocatalytic reaction.

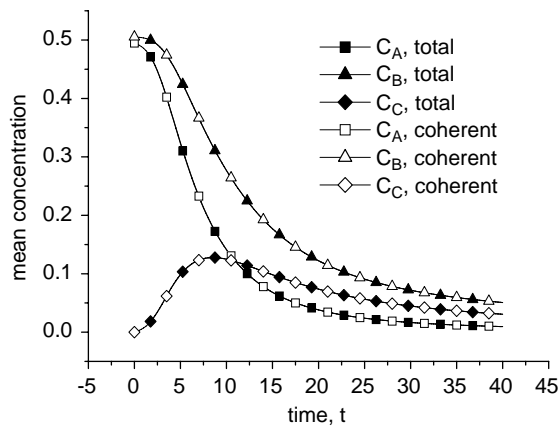


Fig. 15. Mean concentrations for the autocatalytic reaction.

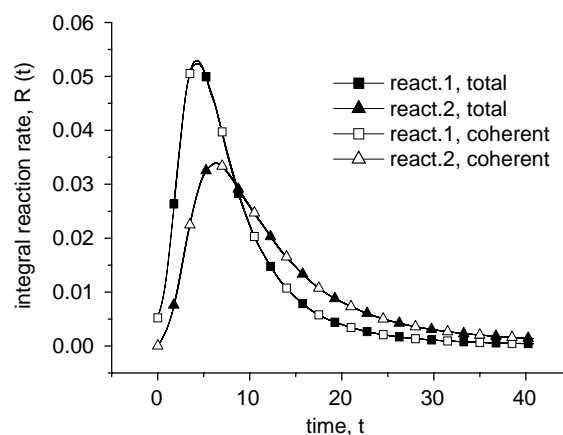


Fig. 16. Integral reaction rates for the autocatalytic reaction.

We find that the highly compressed coherent part of the flow, made of only $0.9\%N$ of the wavelet modes of the total flow but containing most of its kinetic energy, reproduces the mixing properties of the total flow to a large extent. On the other hand, the incoherent part of the flow, containing

the remaining $99.1\%N$ wavelet modes but only very little of the kinetic energy of the flow, causes a diffusional mixing for which the PDF of the concentration field can be modelled using a β -PDF. This result holds, not only for the mixing

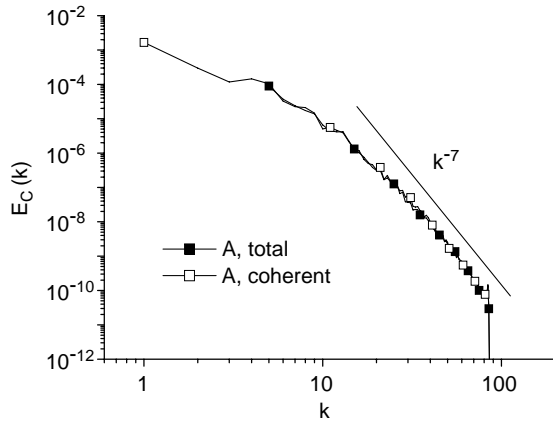


Fig. 17. Scalar energy spectrum at $t = 17.5$ for the autocatalytic reaction (reactive scalar A).

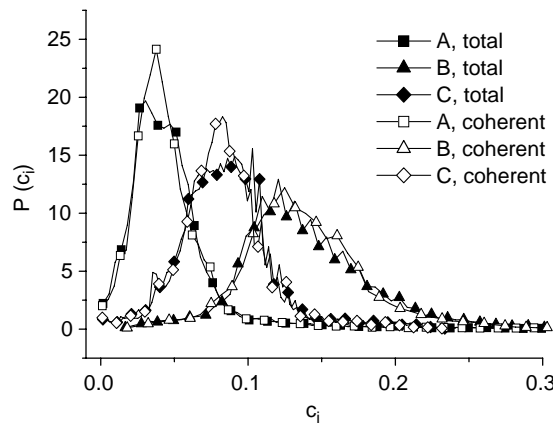


Fig. 18. PDFs of concentrations at $t = 17.5$ for the autocatalytic reaction.

of passive scalars, but also for reactive chemical species with simple as well as multi-step kinetic reaction patterns. In order to compare the mixing dynamics in the total flow and the coherent part, we applied various measures ranging from standard quantities, like the scalar variance and the integral reaction rate, to more intricate ones, like the scalar gradient production which is newly introduced here as a mixing measure.

The successful application of the CVS filter to study mixing and reacting flows constitutes a first step before extending wavelet techniques, namely the CVS method, to model mixing and reaction processes in turbulent flows. In the next step, the flow evolution of the coherent part will be directly computed in an adaptive wavelet basis while the influence of the incoherent background flow will be modelled, as done in Farge and Schneider (2001). This will allow to reduce the memory requirements and the computing costs for high Reynolds numbers, as the adaptive wavelet scheme has linear complexity. Future work will be concerned with projecting also the convection–diffusion–reaction equations onto an orthogonal wavelet basis and computing a small

number of active modes in an adaptive wavelet basis. If the computational cost for simulating the scalar dynamics can be reduced in this way, wavelet methods might facilitate the computation of mixing processes involving species with large Schmidt numbers. Furthermore, it is intended to extend the present work to three-dimensional turbulent flows. Since the CVS filter has already been successfully applied to incompressible three-dimensional flows (Farge et al., 2001; Schneider et al., 2000), it seems reasonable to expect that the present method should also be applicable to study mixing processes in three-dimensional turbulent flows.

Acknowledgements

We acknowledge partial support from the French–German program Procope (contract 01220ZE), the NSF-CNRS-DAAD joint research program (contract 9201), the European SOCRATES exchange program, and the Studienstiftung des deutschen Volkes.

Appendix A. Local gradient production rate

In an incompressible flow, stretching is due exclusively to the strain tensor (Protas et al., 1999; Lapeyre et al., 1999; Lapeyre et al., 2000), which is the symmetric part of the velocity gradient tensor $\nabla \mathbf{v}$. In the decomposition of the velocity gradient tensor into its symmetric and antisymmetric part, $\nabla \mathbf{v} = \mathbf{D} + \mathbf{\Omega}$, we can express \mathbf{D} and $\mathbf{\Omega}$ in terms of the velocity gradient tensor itself and its transpose:

$$\mathbf{D} \equiv \frac{1}{2}(\nabla \mathbf{v} + (\nabla \mathbf{v})^T) \quad \text{strain tensor (symmetric),} \quad (\text{A.1})$$

$$\mathbf{\Omega} \equiv \frac{1}{2}(\nabla \mathbf{v} - (\nabla \mathbf{v})^T) \quad \text{vorticity or spin tensor (antisymmetric).} \quad (\text{A.2})$$

An explicit evaluation of these expressions yields

$$\mathbf{D} = \begin{bmatrix} s_{11} & s_{12} \\ s_{12} & -s_{11} \end{bmatrix}, \quad (\text{A.3})$$

and

$$\mathbf{\Omega} = \begin{bmatrix} 0 & -\omega \\ \omega & 0 \end{bmatrix}, \quad (\text{A.4})$$

where the components are:

$$s_{11} = \partial_x u - \partial_y v, \quad (\text{A.5})$$

$$s_{12} = \partial_x v + \partial_y u, \quad (\text{A.6})$$

$$\omega = \partial_x v - \partial_y u. \quad (\text{A.7})$$

Solving the eigenvalue equation for \mathbf{D} , one obtains the two eigenvectors of the strain tensor

$$\mathbf{d}_1 = \begin{bmatrix} s_{12} \\ s - s_{11} \end{bmatrix}, \quad \mathbf{d}_2 = \begin{bmatrix} -s_{12} \\ s + s_{11} \end{bmatrix} \quad (\text{A.8})$$

with $s = \sqrt{s_{11}^2 + s_{12}^2}$.

They are mutually orthogonal and represent the directions of maximum stretching (\mathbf{d}_1) and maximum compression (\mathbf{d}_2).

Using this kinematic description of the flow, it is possible to describe the evolution of gradients in a concentration field advected by the flow. To study the production of concentration gradient, the gradient vector is separated into magnitude and orientation,

$$\nabla c = \eta \begin{pmatrix} \cos \theta \\ \sin \theta \end{pmatrix}. \quad (\text{A.9})$$

The evolution of its magnitude η depends strongly on the angle between the concentration gradient vector and the second eigenvector \mathbf{d}_2 of the strain tensor (Protas et al., 1999; Lapeyre et al., 1999). In fact, for the instantaneous change of concentration gradient, one finds (Ottino, 1989)

$$\frac{1}{\eta} \frac{d\eta}{dt} = -\mathbf{m}^T \mathbf{D} \mathbf{m} \quad (\text{A.10})$$

$$= \frac{1}{2} s \cos 2\alpha \quad (\text{A.11})$$

with $\mathbf{m} = \nabla c / |\nabla c|$ and α the angle between the concentration gradient vector ∇c and the compressing eigenvector \mathbf{d}_2 of the strain tensor. In order to get a production rate of concentration gradient that is proportional to the strength of the gradient itself (the production of gradient is most important where the gradient is strongest), we multiply Eq. (A.10) with η and obtain

$$\gamma = \frac{1}{2} \eta s \cos 2\alpha \quad (\text{A.12})$$

the instantaneous local relative production rate of concentration gradient. Here, $\gamma = \gamma(\mathbf{x}, t)$ is a function of space and time, because η , s , and also α are dependent on position in space and on time.

Appendix B. β -PDF

In this work, we use β -PDFs to fit the PDFs of concentration fields (Baldyga, 1989). The β -PDFs are computed according to the following definition:

$$\beta(c) = \frac{c^{a-1}(1-c)^{b-1}}{\int_0^1 x^{a-1}(1-x)^{b-1} dx}, \quad c \in [0, 1] \quad (\text{B.1})$$

with

$$a = \bar{c} \left(\frac{\bar{c}(1-\bar{c})}{\sigma_c^2} - 1 \right) \quad (\text{B.2})$$

and

$$b = (1-\bar{c}) \left(\frac{\bar{c}(1-\bar{c})}{\sigma_c^2} - 1 \right), \quad (\text{B.3})$$

where \bar{c} denotes the mean of the concentration field and σ_c^2 its variance.

Appendix C. Notations

Throughout this work, physical quantities are given as dimensionless variables. They have been non-dimensionalized using the reference quantities shown below.

Notation	Units	Quantity
c_0^*	1 mol m ⁻³	Reference concentration
l_0^*	1 m	Reference length
m_0^*	1 kg	Reference mass
t_0^*	1 s	Reference time

The corresponding dimensional quantities are marked by a star, e.g. ν^* , the kinematic viscosity in m² s⁻¹, and ν the corresponding non-dimensionalized variable given in units of $l_0^{*2} t_0^{*-1}$.

References

- Baldyga, J. (1989). Turbulent mixer model with application to homogeneous, instantaneous chemical reactions. *Chemical Engineering Science*, *44*, 1175–1182.
- Basdevant, C., Legras, B., Sadourny, R., & B eland, M. (1981). A study of barotropic model flows: Intermittency, waves and predictability. *Journal of Atmospheric Science*, *38*, 2305–2326.
- Batchelor, G. K. (1953). *The theory of homogeneous turbulence*. Cambridge: Cambridge University Press.
- Bockhorn, H. (1991). Simulation chemischer Reaktionen in turbulenten Str omungen. *Chemie-Ingenieur-Technik*, *63*, 715.
- Canuto, C., Hussaini, M. Y., Quaternioni, A., & Zang, T. A. (1988). *Spectral methods in fluid dynamics*. Berlin: Springer.
- Cook, A. W., & Riley, J. J. (1998). Subgrid-scale modeling for turbulent reactive flows. *Combustion and Flame*, *112*, 593–606.
- Corsin, S. (1964). The isotropic turbulent mixer: Part II. Arbitrary Schmidt number. *A.I.Ch.E. Journal*, *10*(6), 870–877.
- Daubechies, I. (1992). *Ten lectures on wavelets*. Philadelphia: SIAM.
- Donoho, D. (1993). Unconditional bases are optimal bases for data compression and statistical estimation. *Applied Computational Harmonic Analysis*, *1*, 100.
- Donoho, D., & Johnstone, I. (1994). Ideal spatial adaption via wavelet shrinkage. *Biometrika*, *81*, 425–455.
- Farge, M. (1992). Wavelet transforms and their application to turbulence. *Annual Review of Fluid Mechanics*, *24*, 395–457.
- Farge, M., Azzalini, A., Mahalov, A., Nicolaenko, B., Tse, F., Pellegrino, G., & Schneider, K. (2002). Vortex tubes in shear-stratified turbulence. In K. Bajer, & K. Moffat (Eds.), *IUTAM symposium on tubes, sheets and singularities*. Dordrecht: Kluwer Academic Press, accepted for publication.
- Farge, M., Pellegrino, G., & Schneider, K. (2001). Coherent vortex extraction in 3D turbulent flows using orthogonal wavelets. *Physical Review Letters*, *87*, 054501.
- Farge, M., & Rabreau, G. (1988). Transform ee en ondelettes pour d etecter et analyser les structures coh erentes dans les  coulements turbulents

- bidimensionnels. *Comptes Rendus de l'Academie Sciences Paris, Serie II*, 307, 1479–1486.
- Farge, M., & Schneider, K. (2001). Coherent vortex simulation (CVS), a semi-deterministic turbulence model using wavelets. *Flow, Turbulence and Combustion*, 66(4), 393–426.
- Farge, M., Schneider, K., & Kevlahan, N. (1999). Non-Gaussianity and coherent vortex simulation for two-dimensional turbulence using an adaptive orthogonal wavelet basis. *Physics of Fluids*, 11(8), 2187–2201.
- Farge, M., Schneider, K., Pellegrino, G., Wray, A., & Rogallo, B. (2000). CVS decomposition of three-dimensional homogeneous turbulence using orthogonal wavelets. *Proceedings of the 2000 summer program, Center for Turbulence Research, Nasa Ames and Stanford University* (pp. 305–317).
- Ferziger, J. H. (1995). Large eddy simulation. In T. B. Gatski, M. Y. Hussaini, & J. L. Lumley (Eds.), *Simulation and modeling of turbulent flows*. New York: Cambridge University Press.
- Flohr, P., & Vassilicos, J. C. (1997). Accelerated scalar dissipation in a vortex. *Journal of Fluid Mechanics*, 348, 295–317.
- Frisch, U. (1995). *Turbulence, the legacy of A.N. Kolmogorov*. Cambridge: Cambridge University Press.
- Gerlinger, W., Schneider, K., Falk, L., & Bockhorn, H. (2000). Numerical simulation of the mixing of passive and reactive scalars in two-dimensional flows dominated by coherent vortices. *Chemical Engineering Science*, 55, 4255–4269.
- Grossmann, A., & Morlet, J. (1984). Decomposition of Hardy functions into square integrable wavelets of constant shape. *SIAM Journal of Mathematical Analysis*, 15, 723–736.
- Im, H., Lund, T., & Ferziger, J. (1997). LES of turbulent front propagation with dynamic subgrid models. *Physics of Fluids*, 9(12), 3826–3833.
- Lapeyre, G., Hua, B. L., & Klein, P. (2000). Dynamics of tracer gradient orientation in 2D flows. In C. Dopazo et al. (Eds.), *Advances in turbulence VIII* (pp. 237–248). Barcelona: CIMNE.
- Lapeyre, G., Klein, P., & Hua, B. L. (1999). Does the tracer gradient vector align with the strain eigenvectors in 2D turbulence?. *Physics of Fluids*, 11(12), 3729–3737.
- Legras, B., Santangelo, P., & Benzi, R. (1988). High resolution numerical experiments for forced two-dimensional turbulence. *Europhysics Letters*, 5, 37–42.
- Lesieur, M. (1997). *Turbulence in fluids*. Dordrecht: Kluwer Academic Publishers.
- Louis, A. K., Maaß, P., & Rieder, A. (1998). *Wavelets. Theorie und Anwendungen*. Wiesbaden: Teubner.
- Mallat, S. (1997). *A wavelet tour of signal processing*. New York: Academic Press.
- Meneveau, C. (1991). Analysis of turbulence in the orthogonal wavelet representation. *Journal of Fluid Mechanics*, 232, 469–520.
- Moin, P., Pierce, C., & Pitsch, H. (2000). Large eddy simulation of turbulent, nonpremixed combustion. In C. Dopazo et al. (Eds.), *Advances in turbulence VIII* (pp. 385–392). Barcelona: CIMNE.
- Ottino, J. M. (1989). *The kinematics of mixing: Stretching, chaos, and transport*. Cambridge: Cambridge University Press.
- Ottino, J. M. (1990). Mixing, chaotic advection, and turbulence. *Annual Review of Fluid Mechanics*, 22, 207–253.
- Protas, B., Babiano, A., & Kevlahan, N. (1999). On geometrical alignment properties of two-dimensional forced turbulence. *Physica D*, 128, 169–179.
- Schneider, K., Farge, M., Pellegrino, G., & Rogers, M. (2000). CVS filtering of 3D turbulent mixing layers using orthogonal wavelets. *Proceedings of the 2000 summer program, Center for Turbulence Research, Nasa Ames and Stanford University* (pp. 319–330).
- Schneider, K., Kevlahan, N., & Farge, M. (1997). Comparison of an adaptive wavelet method and nonlinearly filtered pseudo-spectral methods for two-dimensional turbulence. *Theoretical and Computational Fluid Dynamics*, 9(3/4), 191–206.